High-Efficiency Screen-Printed p-Si Interdigitated Back Contact Cells: Fabrication and Analytical Characterization

Pi-Yu Hsin, Yin-Wei Peng, and Jon-Yiew Gan

***Abstract*—In this paper, we report on the fabrication and analytical characterization of the screen-printed p-Si interdigitated back contact (IBC) cells with the conversion efficiency of 20.08%, with open-circuit voltage of 645 mV, short-circuit current density of 40.15 mA/cm^2, and fill factor of 77.51%. The cell performance has also been confirmed with the analytical calculation based on the electrical properties measured. It also shows that, with the proper emitter design, the open-circuit voltage of 680 mV and conversion efficiency of 22% are readily attainable for the screen-printed p-Si IBC cell. Compared with the screen-printed IBC cells, the passivated emitter and rear "contact" cell may perform equivalently well, provided that any improvement on $S_{\rm eff}$ of the front surface does not compromise the light absorption and emitter resistance of the cell.**

***Index Terms*—Interdigitated back contact (IBC), p-type, screen printed, silicon solar cell.**

I. Introduction

OWING to the simplicity of screen printing and Al back-surface-field (Al-BSF), p-Si crystalline solar cells have dominated the market ever since the cell was commercialized. The cell has recently been improved substantially by deploying some innovative technology in the cell fabrication, namely the passivated emitter and rear "contact" (PERC). Compared with the conventional cells, PERC cell includes two modifications: one is the lower doping of the front n^+-emitter, and the other is the smaller area fraction of the rear Al-BSF. Various technologies have been developed to achieve the goals including the etch-back and reduced doping for emitters, and the laser ablation and screen-printed etch for rear contacts. Both modifications can effectively suppress the surface recombination, and so the cell's open-circuit voltage $V_{\rm OC}$ increases. At present, PERC cells made on both the multicrystalline and monocrystalline wafers have been reported with the conversion efficiency η over 20% [1]–[7]. The success of PERC cell also raises interests in seeking more compatible technology and cell design that can further improve the cell performance.

Manuscript received March 1, 2017; revised May 16, 2017; accepted June 18, 2017. Date of publication July 11, 2017; date of current version August 18, 2017. *(Corresponding author: Pi-Yu Hsin.)*

The authors are with the Department of Materials Science and Engineering, National Tsing Hua University, Hsinchu 30013, Taiwan (e-mail: backyhsin@gmail.com; yinweipeng2@gmail.com; jygan@mx.nthu.edu.tw).

Color versions of one or more of the figures in this paper are available online at http://ieeexplore.ieee.org.

Digital Object Identifier 10.1109/JPHOTOV.2017.2719582

Among them, the fabrication of p-Si screen-printed interdigitated back contact (IBC) cell has caught much of our attention. IBC has long been regarded as the optimum structure of Si solar cell owing to its several remarkable advantages. First, it eliminates optical shading on the front side so that a higher short-circuit current density $J_{\rm SC}$ can be obtained. Second, the front-surface passivation can be optimized without the constraint of low emitter resistance subjected to the PERC cell. Third, panels with preformed bonding pads can be used in the module assembling because electrodes for both emitters and collectors are on the same backside of IBC cells. This enhances the throughput rate of module assembling and thus reduces the cost of production. Numerous IBC technologies have been reported in the past years and have resulted in cells with record-high efficiency both in the laboratory scale and the commercial production [8]–[14]. Although the fabrication of high-efficiency IBC cells normally uses lithography to define contacts and metal fingers, there are still some reports on the fabrication of IBC cells with the screen printing technology. Woehl *et al*. has reported on the screen-printed n-Si IBC cells [15]. In their work, the cell's emitter was formed with the screen-printed and fired Al fingers, and the contact electrode of n^+-collector was the Ag finger. They recorded the cell with η of 20%. In addition, Dong *et al*. has also reported the full size screen-printed n-Si IBC cells [16]. Their cells were fabricated with the double diffusion using $POCl_3$ and BBr_3, respectively, to form the n^+-collector and p^+-emitter, and screen-printed Ag for both electrodes. The cell performance was recorded with η of 19.65%. Besides, Scardera *et al*. also made screen-printed dopant paste IBC cells with efficiency up to 21% [17]. Results from above-mentioned cases are promising since the cell performance reported is comparable to that of conventional p-Si screen-printed cells, not mentioning η of 22% is projected by these groups when the cell is optimized.

In this paper, we report the characteristics of the screen-printed p-Si IBC cell. It shows that, with the proper emitter design, $V_{\rm OC}$ of 680 mV and η of 22% are readily attainable for the screen-printed p-Si IBC cell, despite the bulk lifetime of p-Si wafer being inferior to that of n-type wafer. Section II describes the fabrication details and specification of cell structure and material properties. For comparison, the cell was fabricated alongside with the PERC cell using the same processing technology. Section III presents the characterization results and analysis of the cell. The characterization includes the measurement of light *I–V* of cells and recombination of various surfaces appeared in

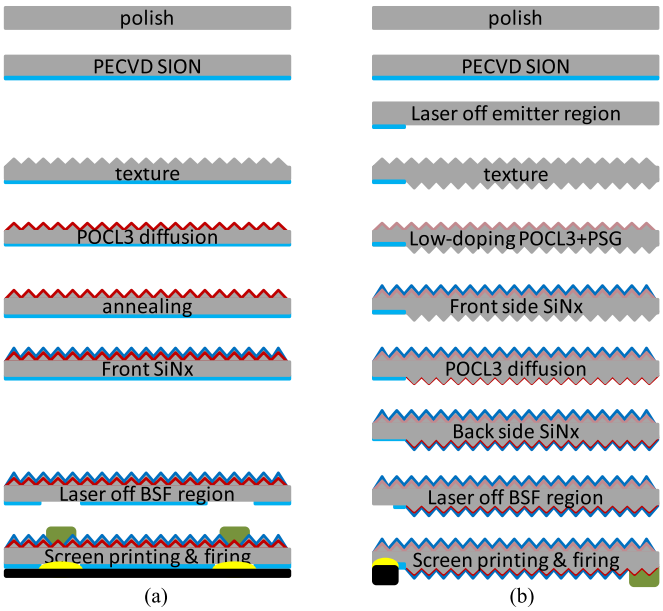

Fig. 1. Comparison of process flows between (a) PERC solar cell and (b) IBC solar cell.

the cell. Instead of using numerical simulation, we present analytical derivations of the open-circuit voltage V_{OC}, short-circuit current I_{SC}, and fill factor FF based on the cell structure. The analysis not only verifies the cell characteristics, but also reveals the importance of emitter recombination in determining the cell performance. A brief conclusion is given in Section IV.

II. Cell Fabrication and Structure

6″ solar grade p-type Cz wafers with thickness of about 200 μm and resistivity around 1 $\Omega \cdot$ cm were used in this study. The bulk lifetime of the wafer, suggested by the vendor, is around 400 μs. Fig. 1 shows the process flow of IBC and PERC cells. As illustrated, the fabrication of IBC cell is a modification of that for the PERC. In the fabrication of IBC cells, wafers were first wet etched to remove saw damage and coated with a plasma enhanced chemical vapor deposition (PECVD) SiON for the backside emitter definition using laser ablation. After the texturization and prefurnace clean, a low-doping $POCl_3$ diffusion was applied to form a blanket emitter on the front surface (180 Ω/square), which was capped immediately with PECVD SiN_x without the removal of phosphosilicate glass (PSG) to attain low surface recombination velocity. A high-doping $POCl_3$ was then applied to form the backside emitter (70 Ω/square), followed with another PECVD coating, and then a BSF definition using laser ablation. Finally, Al and Ag fingers and busbars were fabricated on the back surface with the screen printing and belt-furnace firing. In the firing, the BSF is also formed with Al paste simultaneously. For the PERC cell fabrication, the same high-doping $POCl_3$ was used to form the front n^+-emitter (70 Ω/square), and the backside BSF structure was fabricated with the same laser ablation. Compared with the PERC process, IBC fabrication requires two additional steps in order to define the front floating emitter and backside emitter separately.

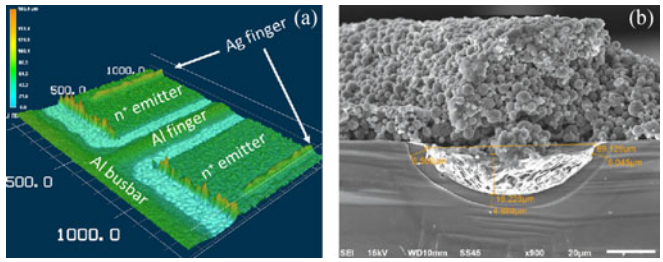

Fig. 2. (a) 3-D surface scan over the IBC grids near the edge of one Al busbar. (b) Cross-section view SEM micrograph of 6 μm thick BSF formed after firing under the aluminum finger at the laser ablation region.

The PERC cell is fabricated on 6″ square wafers with the 3-busbar configuration. The optimized finger and busbar design typically result in an optical shading of about 5%. In contrast, the IBC cell was a 10 cm $\times$ 10 cm square cell in order to match the setup of cell measurement. It uses two Ag and three Al interchanged busbars that are 1.5 mm wide with a pitch of 2.5 cm. The interdigitated Al and Ag fingers of 2.3 cm long are formed between two neighboring busbars. Fig. 2(a) shows the three-dimensional (3-D) surface scan over the IBC grids near the edge of one Al busbar. In the figure, the pitch between two Ag fingers is 1200 μm wherein includes two halves of n^+-emitter region and a SiON passivation region in between. The n^+-emitter is 850 μm wide that leaves the width of SiON region of 350 μm. The gap between Al busbar and the emitter edge is 250 μm, so is the distance from the tip of Ag finger to the emitter edge. The Ag finger lying on the top of emitter is 80 μm wide and 39 μm high. Fig. 2(b) shows the cross-section view of the Al finger and BSF underneath. The shape of Al finger appears to be triangular ($C_{Al} = 1/2$) after firing with the base width of 150 μm and height of 30 μm. The ablated elliptic trough is about 70 μm wide and 16 μm deep, and after sintering, a uniform BSF of 6 μm thickness is formed around the elliptic circumference, corresponding to an Al-to-BSF contact of about 100 μm long.

Owing to the periodic array of metal grids, a unit cell bounded with busbars and fingers is used in the subsequent analysis. The dimension of unit cell adopted in this work is 1200 μm wide and 2.5 cm long; i.e., the pitch between two Ag fingers and that between two neighboring busbars, respectively. For clarity, Table I summarizes all parameters aforementioned, along with the electrical properties of materials characterized with 4-point probing. Note that the resistivity of Al finger ($2.5 \times 10^{-5}\ \Omega \cdot$ cm) is about ten times higher than that of the pure Al. It is resulted from the poor electrical conductivity among Al particles owing to the firing and/or paste composition was not optimized. To facilitate the subsequent analysis, the table also includes the specific contact resistance of Ag/n^+-emitter and Al/BSF that are excerpted from [18] to be 1.5 and 5 m$\Omega \cdot$ cm^2, respectively.

III. Results and Analysis

A. Cell Performance and Effective Surface Recombination Velocity

Cell performance was measured in a commercial solar simulator BERGER Lichttechnik cell testing system using AM1.5G

TABLE I
DISTRIBUTION OF SATURATION CURRENT

Term	Magnitude
W_b, p-base ($\approx$ cell) thickness (μm)	200
τ_b, p-base bulk lifetime (μs)	400
ρ_b, p-base resistivity ($\Omega \cdot$ cm)	0.5–2
W_{Bar}, busbar width (μm)	1500
L_c and L_f, length of unit cell and finger (cm)	2.5 and 2.3
W_c and W_E, width of unit cell and emitter (μm)	1200 and 850
W_{BSF} and t_{BSF}, BSF width and thickness (μm)	100 and 6
W_{Al} and t_{AI}, Al finger width and thickness (μm)	150 and 30
C_{Al}, correction of Al finger cross-section area	1/2
W_{Ag} and t_{Ag}, Ag finger width and thickness (μm)	80 and 39
ρc, AI/BSF specific contact resistance ($\Omega \cdot \text{cm}^2$)	5×10^{-3}*
$\rho_{c,\text{Ag}}$, Ag/n+ emitter specific contact resistance ($\Omega \cdot \text{cm}^2$)	1.5×10^{-3}*
ρ_{Al}, Al finger resistivity ($\Omega \cdot$ cm)	2.5×10^{-5}
ρ_{Al} Ag finger resistivity ρ_{Al} ($\Omega \cdot$ cm)	2.82×10^{-6}
$R_{\square,E}$ $n+$-emitter sheet resistance ($\Omega/\square$)	70

*Ref. [12].

light source for both the IBC and PERC cell. The measurement on PERC cell gave rise to an energy conversion efficiency of 19% that includes V_{OC} of 639 mV, J_{SC} of 37.83 mA/cm^2, and FF of 78.56%. In the measurement of IBC cell, emitter busbars (Ag) of IBC cells were soldered to facilitate electrical connection, as illustrated in Fig. 3(a) and (b). The cell characteristics measured under such a configuration are also shown in Fig. 3(c), which suggests a cell efficiency of 20.08%, V_{OC} of 645 mV, J_{SC} of 40.15 mA/cm^2, and FF of 77.51%. In addition, the shunt resistance R_{SH} and series resistance R_S of IBC cells were also measured to be 3.25 k$\Omega \cdot$ cm^2 and 0.69 $\Omega \cdot$ cm^2, respectively. Compared with that of PERC cell, the efficiency of IBC cell is about 1% higher, which is obviously resulted from the higher J_{SC} of IBC cell.

Besides the cell performance, surface recombination has also been evaluated independently through the lifetime measurement. This includes the recombination at the front floating n-emitter (FFE), back n$^+$-emitter, Al-BSF, and SiN$_x$ passivated p-base surface that is between the last two on the back surface. To characterize, they were prepared separately on blanket wafers using the same process of cell fabrication and tested with Sinton WCT120. Fig. 4 shows the typical lifetime data τ_{eff} measured from the SiN$_x$ and FFE-passivated wafers at the excess carrier concentration (Δn) of 1×10^{15} cm^{-3} [19]. For comparison, results before and after firing are presented, and FFE-passivated wafers without and with PSG on the wafer (FFE + SiON and FFE + PSG + SiON) are also included. Since FFE + PSG + SiON wafers generally appear with larger lifetime, they were adopted in the cell fabrication.

The corresponding effective surface recombination velocity S_{eff} was then derived with the following equation [20]:

$$\frac{S_{\text{eff}}}{W_b/2} = \frac{1}{\tau_{\text{eff}}} - \left(\frac{1}{\tau_{\text{SRH}}} + \frac{1}{\tau_{\text{Auger}}}\right) = \frac{1}{\tau_{\text{eff}}} - \frac{1}{400\ \mu\text{s}} \quad (1)$$

where W_b is the wafer thickness. The conversion is legitimate since the wafer thickness ($W_b = 200\,\mu$m) is much less than the diffusion length ($L_n = 1039\,\mu$m), and S_{eff} is less than the diffusion velocity ($D_n/W_b = 1350$ cm/s). These conditions ensure

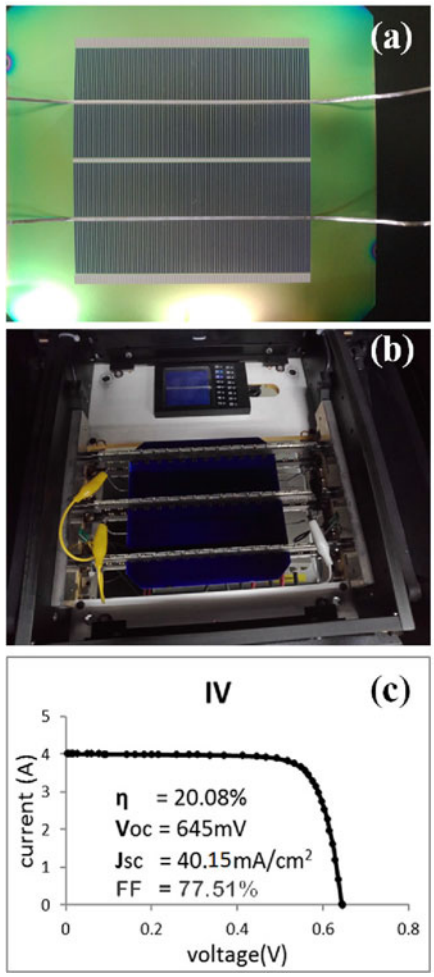

Fig. 3. Cell performance under BERGER Lichttechnik cell testing system. The effective area is 100 cm^2. (a) Back side of the IBC cell. (b) The measurement stage. (c) *I–V* curve of the IBC cell.

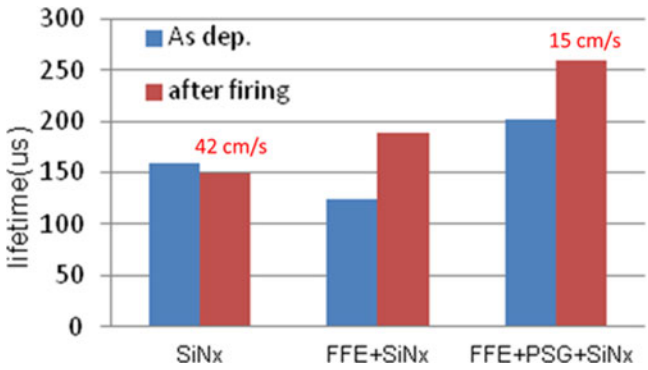

Fig. 4. Comparison of lifetime data measured under Sinton WCT120 at excess carrier concentration of 1×10^{15} cm^{-3} with different surface passivation processes.

uniform distribution of excess carriers across the wafer in the lifetime measurement. After firing, S_{eff} of SiN$_x$-passivated and FFE-passivated with PSG is shown to be 42 and 15 cm/s, respectively. Other S_{eff} with different surface passivations is derived in the same way, and presented in the second column of Table II. Note that S_{eff} of n$^+$-emitter is about 23 times higher than that of the front floating emitter because of the high doping effect. For

TABLE II
EFFECTIVE SURFACE RECOMBINATION VELOCITY AND EQUIVALENT SATURATION CURRENT DENSITY

Source	S_{eff} and W_b/τ_b (cm/s)	Equivalent J_o(fA/cm^2)	Area fraction in IBC	J_o in IBC (fA/cm^2)
Bulk recombination	50	80	1.00	80
Front floating emitter (FFE)	15	24	1.00	24
SiON-capped	42	67.2	270/1200	15
BSF SiN_x-capped	62.5	100	100/1200	8
Heavily doped emitter	345	552	850/1200*	391

*Including the Ag-contacted emitter.

BSF wafers, the lifetime measurement was performed on the wafers after Al was stripped off. Despite that, S_{eff} was derived to be 62.5 cm/s that is also in good agreement with the value reported by others [21].

With the detail information of the cell structure and electrical properties, it is possible to verify the cell performance by analyzing independently the open-circuit voltage V_{OC}, short-circuit current J_{SC}, and fill factor FF. The analysis is presented in the sections as follows.

B. Analysis of V_{OC}

The open-circuit voltage is related to the sum of recombination occurred in the cell. Assuming low-level injection ($\Delta n < N_A \approx 1 \times 10^{16}\,\text{cm}^{-3}$) and negligible recombination in the space-charge region for the IBC cell under the open-circuit condition V_{OC} can be expressed as

$$V_{\text{OC}} = \frac{k_B T}{q} \ln\left(\frac{J_{\text{SC}}}{J_{o,\text{cell}}} + 1\right) \approx \frac{k_B T}{q} \ln\left(\frac{J_{\text{SC}}}{J_{o,\text{cell}}}\right) \quad (2)$$

where $J_{o,\text{cell}}$ is the saturation current density of the cell that is related to the bulk recombination and surface recombination with

$$J_{o,\text{cell}} = \frac{qn_i^2}{N_A}\left(\frac{W_b}{\tau_b} + \sum A_i S_{\text{eff},i}\right) = \sum A_i J_{o,i}. \quad (3)$$

In the equation, W_b/τ_b and $S_{\text{eff},i}$ are the value listed in the second column of Table II. $J_{o,i}$ and A_i are the equivalent saturation current density and area fraction of each component shown in columns 3 and 4, respectively. Their product $(A_i \times J_{o,i})$ is listed in the last column of the table. By summing up the last column, $J_{o,\text{cell}}$ is derived to be 518 fA/cm^2. Substituting $J_{o,\text{cell}}$ and the measured J_{SC} (40.15 mA/cm^2) into (2), an open-circuit voltage of 649 mV is derived at 300 K that deviates from the value of measurement (645 mV) only by 4 mV. The slightly higher value of calculated V_{OC} is likely caused by assuming the same S_{eff} for the Ag-contacted and the SiN_x-passivated n^+-emitter, despite S_{eff} of the former is higher. The assumption underestimates J_o of n^+-emitter and therefore results in higher V_{OC}.

It is interesting to note that J_o associated with the Al-BSF appears to be the lowest in the table, which is about 8 fA/cm^2 when weighted with the area fraction. Assume that the other recombination of the cell can be ignored and only consider the recombination of the Al-BSF, this is amount to having V_{OC} over 750 mV. Although the above-mentioned saying is highly hypothetical, it does show the importance of incorporating Al-diffused BSF into the p-type IBC cell fabrication. Table II also presents the dominant recombination to be the one from the n^+-emitter; it counts about 75% of $J_{o,\text{cell}}$ and overwhelms the others in determining V_{OC}. Since the PERC and IBC cell were fabricated with the same n^+-emitter, it thus explains the similar V_{OC} observed in both cells. Significant reduction of the recombination from n^+-emitter is possible; for example, using the polysilicon tunneling emitter that has been reported with J_o as low as 10 fA/cm^2 [22], [23]. When this is applied to our IBC cell, the open-circuit voltage should be over 680 mV. Such a replacement is very tempting, as it only needs to add the polysilicon deposition in current IBC cell fabrication process. In contrast, polysilicon emitter may not be so beneficial to PERC cell because the high absorption of polysilicon can reduce J_{SC} substantially.

As illustrated in the table, the bulk recombination may become the largest term once the recombination of n^+-emitter is effectively reduced. It, however, can be suppressed by using wafer that is thinner and/or with higher bulk lifetime. Putting all the improvements together, p-type IBC cells with V_{OC} over 700 mV are quite feasible in the near future.

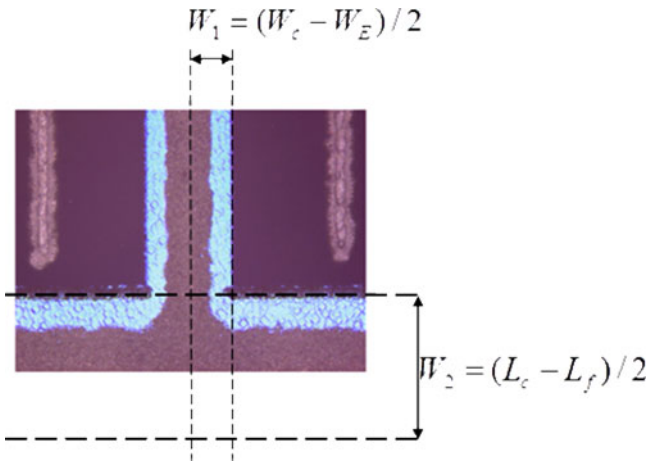

Fig. 5. Top view of the Al and Ag fingers near the Al busbar.

C. Analysis of J_{SC}

The short-circuit current is the flux of excess minority carriers collected by the junction. Since the n^+-emitter is thin and located on the back surface of IBC cell, J_{SC} can be well approximated with the flux of excess electrons collected from the p-base region. The flux is nevertheless three-dimensional and often derived with numerical simulations [24]. To simplify the analysis, the unit cell is divided into three regions in which excess electron collection can be approximated with one-dimensional flux in series. Fig. 5 shows these regions near the edge of Al busbar. The first region is the base region right on the top of n^+-emitter, the second one is that between the edge of n^+-emitter and the center of Al finger, and the third one is the base region ranging

TABLE III
PARAMETERS USED IN THE DERIVATION OF J_{SC} LOSS IN IBC CELLS

Source	S_{eff} in CP (cm/s)	L_{eff}/W (μm/μm)	Area fraction in IBC	J_{SC} loss in IBC (%)
Vertical collection above emitter	15	196.5/200	850 × 0.93/1200*	1.15
Lateral collection from Al finger to emitter	0	173.4/175	350/1200	0.78
Lateral collection from Al busbar to emitter	0	774.4/1000	1000/25 000	0.97

*Length ration = 2.325 cm/2.5 cm = 0.93.

from the tip of n^+-emitter to the centerline of Al busbar that is schematically drawn in the figure.

Photogenerated electrons of each region are assumed first to diffuse vertically from the front surface toward the back surface. In the first region, electrons are directly collected by the n^+-emitter. In the other two regions, electrons have to make additional diffusion that is laterally along the back surface to the n^+-emitter in order to make their contribution of J_{SC}. For the downward vertical diffusion, the corresponding J_{SC} can be expressed as

$$J_{SC} = q\int_0^{W_b}\left[\int_0^{\lambda_{Eg}} G_\lambda(x)d\lambda\right]\mathrm{CP}(x)dx$$
$$= q\int_0^{W_b} G(x)\mathrm{CP}(x)dx = qG_{avg}\int_0^{W_b}\mathrm{CP}(x)dx = qG_{avg}L_{eff} \quad (4)$$

where $G_\lambda(x)$ is the generation rate at the depth of x caused by the absorption of photon flux with the wavelength of λ. CP(x) is the electron collection probability that can be expressed as

$$\mathrm{CP}(x) = \frac{[(D_n/L_n)+S_{eff}]\,e^{x/L_n}+[(D_n/L_n)-S_{eff}]\,e^{-x/L_n}}{[(D_n/L_n)+S_{eff}]\,e^{W_b/L_n}+[(D_n/L_n)-S_{eff}]\,e^{-W_b/L_n}}. \quad (5)$$

Here, S_{eff} is the effective surface recombination of the front floating emitter (15 cm/s) for the vertical diffusion. Equation (4) further approximates the generation rate with a constant of G_{avg} to simplify the integration. The assumption overestimates J_{SC} of which effect has been confirmed with numerical calculation. Nevertheless, the assumption gives a convenient physical quantity, the effective collection length L_{eff}, that can be used to estimate quantitatively the collection efficiency. The latter is defined as the ratio of L_{eff} to the actual collection length, which is the base thickness W_b in the vertical diffusion. Similar approach has also been used to derive the corresponding L_{eff} of the lateral diffusion by substituting the appropriate collection length W and setting S_{eff} to zero since the flow is balanced at the centerline of Al finger and busbar.

Table III summarizes the results of calculation. For the vertical diffusion, L_{eff} is calculated to be 196.5 μm that means a collection efficiency of 98.25%, or equivalently a collection loss of 1.75%. Weighted with the emitter area, the first region causes a J_{SC} loss of 1.15% to the cell as illustrated in the fifth column of the table. For the second and third regions, L_{eff} corresponding to the lateral diffusion is 173.4 and 774.4 μm, respectively. By adding up with the loss of vertical diffusion, the J_{SC} loss of these two regions is 0.78% and 0.97%, respectively. Collection loss of these two regions is commonly referred to the electrical shading effect [25]. As shown, they contribute less to the J_{SC} loss of the cell compared to that of the first region owing to the smaller area fraction. Summing up the collection loss, it shows a J_{SC} loss of 2.90% owing to the collection of electrons with the back n^+-emitter.

To calculate J_{SC}, it still needs to know the generation rate G_{avg}. Assuming a negligible transmission of the back surface, it can be expressed as

$$G_{avg} = \frac{(1-R_{avg})}{W_b}\int_0^{\lambda_{Eg}} F(\lambda)d\lambda. \quad (6)$$

Here, the integration is the total photon flux available for the photogeneration in silicon that is about 2.738×10^{17} cm$^{-2}\cdot$s^{-1} according to the AM1.5G spectrum. R_{avg} is the overall fraction of the incident spectrum being reflected at the front surface, which is typically about 3% for the SiN_x coated and texturized front surface [26]. Adding up the reflection and collection loss (5.90% in total), and using the total photon flux of AM1.5G spectrum, it gives rise to J_{SC} of 41.22 mA/cm^2 for the cell. This is about 1.07 mA/cm^2 higher than that measured (40.15 mA/cm^2). The deviation is primarily caused by the assumption of uniform generation rate. It underestimates the collection loss near the front surface where the generation is the highest and yet the collection efficiency is the least. By including the nonuniform generation, the numerical calculation indicates the total collection loss may increase from 2.90% to 4.34% that in turn reduces J_{SC} to 40.6 mA/cm^2, which is closer to the measured value. There are other possible errors including the solar spectrum used in the test, the quality of the antireflection coating and texturization, and the transmission of the back surface. Nevertheless, these effects are minor compared with the assumption of uniform generation.

It is also interesting to note that, from the numerical calculation, the collection loss of PERC cell is considerably less than the loss of optical shading. According to our design, the latter is about 5%, and the total J_{SC} loss of PERC cell is about the same as that of IBC cell. That implies both cells are supposed to have similar J_{SC}. It is, however, in conflict with our experiment wherein J_{SC} of PERC cell is shown to be much lower than that of IBC cell. Evidently, there is additional loss mechanism associated with PERC cell that remains to be identified.

As illustrated, the collection loss associated with the vertical diffusion is the dominant one in IBC cell. The term appears to be very susceptible to S_{eff} of the front surface. For example, by applying S_{eff} with 345 cm/s in (5), L_{eff} is then reduced to 177.78 μm that, in turn, causes a collection loss of 11.1% for the vertical diffusion, and a total collection loss of 12.85% of the cell. Evidently high S_{eff} of the front surface not only hurts the open-circuit voltage, but also degrades J_{SC} as well. Various combinations of S_{eff}, τ_b, and W_b have been tried to optimize the

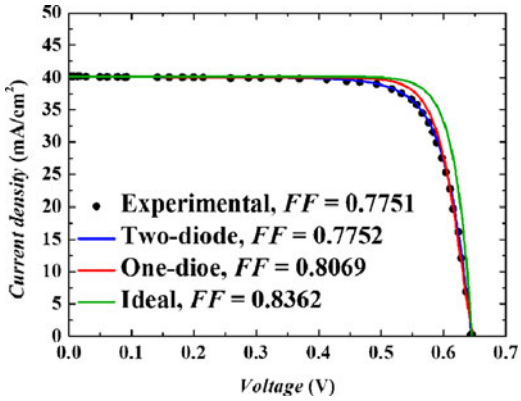

Fig. 6. Experimental and fitting *IV* curves using one-diode and two-diode equations.

collection efficiency. Nevertheless, further improvement of $J_{\rm SC}$ appears to be quite challenging. Numerical calculation indicates that an increase of 1 mA/cm^2 over the present $J_{\rm SC}$ may require a hardly achievable setting of $S_{\rm eff}$, τ_b, and W_b with current technology. Considering the high generation of the front surface, it is, however, noted that additional enhancement of $J_{\rm SC}$ is feasible with low $S_{\rm eff}$.

Note that n^+-emitter is implemented at the front surface of PERC cell. It is, thus, apparent that the high $S_{\rm eff}$ of the front n^+-emitter (345 cm/s) with the high generation rate nearby is the additional loss mechanism of PERC cell. $S_{\rm eff}$ of the front surface can be suppressed by lowering the doping level of emitter; consequently, current high-end PERC cells have used selective emitter with higher sheet resistance ($\geq 100\ \Omega$/square) to improve both $V_{\rm OC}$ and $J_{\rm SC}$ [27].

D. Analysis of FF

Fill factor is a measure of squareness of light current–voltage curve that is generally modeled as [28]

$$J = J_{\rm SC} - J_{o,1}\left[\exp\left(\frac{q(V+JR_S)}{k_BT}\right)-1\right] - J_{o,2}\left[\exp\left(\frac{q(V+JR_S)}{2k_BT}\right)-1\right] - \frac{V+JR_S}{R_{\rm SH}}. \quad (7)$$

In the equation, $J_{o,1}$ describes recombination currents in the quasi-neutral bulk and the cell surfaces, i.e., the sum of the last column in Table I. $J_{o,2}$ primarily denotes SRH recombination in the space charge regions of the cell that is ignored in the calculation of $V_{\rm OC}$. Based on the equation, three light *I–V* curves were derived and plotted in Fig. 6. In the figure, the ideal curve is derived by ignoring the $J_{o,2}$ and $R_{\rm SH}$ terms of the equation, and set R_S to zero. The one-diode curve ignores the $J_{o,2}$ term only, but sets R_S and $R_{\rm SH}$ with the measured value ($0.69\,\Omega\cdot$cm^2, $3.25\,$k$\Omega\cdot$cm^2). The two-diode curve is the fit to the experiment light *I–V* with the full equation and the best setting of $J_{o,2}$ that is 4.08×10^{-8} A/ cm^2. As illustrated, the squareness of curve degrades, as more parasitic terms are included. Compared the one-diode curve with the ideal one, the degradation is mainly resulted from the series resistance effect that lowers FF by about 2.94% absolute. Including the $J_{o,2}$ effect, FF of the two-diode curve is further reduced by about 3.17% absolute from that of the one-diode curve.

Evidently, the lower FF of the two-diode curve has to do with the value of $J_{o,2}$ derived. To estimate the effect, let $J_{\rm mp}$ and $V_{\rm mp}$ be the current and voltage of the one-diode curve at the maximum power point, which is 38.19 mA/cm^2 and 547 mV, respectively, and ΔJ be the current induced by the $J_{o,2}$ term in the equation. Then, the loss of FF can be approximated with $\Delta J(V_{\rm mp})/2J_{\rm mp}$, which is about 3.4%. The latter expression also suggests the FF loss is directly proportional to the value of $J_{o,2}$. According to SRH recombination, $J_{o,2}$ can be evaluated from the bulk lifetime with the depletion width at zero bias. Using the bulk lifetime measured ($400\ \mu$s) and depletion width ($\sim$360 nm) derived from the doping level, $J_{o,2}$ is about 6.8×10^{-11} A/ cm^2 that is about 600 times lower than that derived from the fitting. It is apparent that additional recombination centers may have been introduced to the junction in the cell fabrication, and yet they were not detected in the lifetime measurement aforementioned. Greulich *et al.* [29] have also observed similar effect that, after Ag plating, $J_{o,2}$ increases, and pseudo fill factor decreases accordingly. Although further verification is still needed, electronic defects introduced during the Ag contact firing very likely is the cause. Since the contamination is resulted from the firing process, effective suppression of $J_{o,2}$ may be realized through the adjustment of the composition of Ag paste and the firing parameters.

As stated above, series resistance is the other major cause of FF loss. It consists of the emitter resistance and base resistance encountered, respectively, by the electron current and hole current, and the resistance of Ag and Al fingers. Owing to the distributed characteristic of carrier flow, the series resistance is evaluated with the sum of power loss of each component:

$$R_S \approx \sum_i \frac{P_{{\rm loss},i}/A_{\rm cell}}{J^2} = \sum_i \frac{P_{{\rm loss},i}}{A_{\rm cell}\cdot J^2} = \sum_i R_i \quad (8)$$

where $P_{{\rm loss},i}$ is the power loss caused by component *i*, $A_{\rm cell}$ is the area of unit cell, *J* is the current density of the cell, and R_i in the unit of $\Omega\cdot$cm^2 is the contribution of each component to the cell's series resistance. Note that R_i is independent of the current density used since the detail expression of $P_{{\rm loss},i}$, as illustrated below, also contains the same J^2 term. Most of the detail expressions of $P_{{\rm loss},i}$ have been reported elsewhere [30], and were used in this work with a slight modification according to the geometry of the cell. Most modifications, although physically sound, show only negligible differences in numerical result, except the one caused by the hole current near the tip of the Al finger. Fig. 7 shows schematically the base region near one Al finger's tip. Since the width of Al finger contact ($80\ \mu$m) is much smaller than that of the unit cell ($1200\ \mu$m), hole current to be collected by the Al tip is, therefore, not uniform so that current spreading effect has to be considered in deriving the power loss. To calculate, the region of current spreading is first assumed to be the area bounded with the cell width and the distance between the center of Ag busbar and the Al tip; i.e., the square illustrated in the figure. Second, the current at the location *r* away from the center of Al tip is approximated with

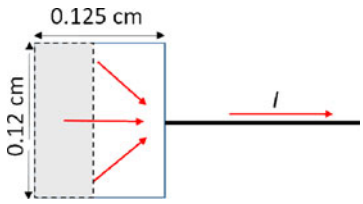

Fig. 7. Schematic of current flow from the middle of the Ag busbar to the tip of Al finger.

TABLE IV
SUMMARY OF SERIES RESISTANCE COMPONENTS

Source	Resistance (Ω·cm^2) Total = 0.5837
Al and Ag contact resistance	0.078
Al finger series resistance	0.25
Ag finger series resistance	0.02
Base series resistance	0.06
Emitter series resistance	0.084
Spreading resistance at Al finger tip	0.0917

a centripetal flow $I(r)$. Then, the spreading resistance R_{spread} is

$$\begin{aligned} R_{\text{spread}} &= \frac{\int_{r_{Al}}^{r_{\text{tip}}} I(r)^2 \cdot \frac{\rho_b dr}{\pi r W_b}}{A_{\text{cell}} \cdot J^2} \\ &= \frac{\int_{r_{Al}}^{r_{\text{tip}}} \left(\int_r^{r_{\text{tip}}} J\pi r dr\right)^2 \cdot \frac{\rho_b dr}{\pi r W_b}}{A_{cell} \cdot J^2} \\ &= \frac{\int_{r_{Al}}^{r_{\text{tip}}} \left(\int_r^{r_{\text{tip}}} \pi r dr\right)^2 \cdot \frac{\rho_b dr}{\pi r W_b}}{A_{\text{cell}}} \end{aligned} \tag{9}$$

where r_{tip} is the radius of a semicircle of which area is equal to that of tip region, and r_{Al} is one half of the Al contact width. Despite the square being approximated with a semicircle, the error is believed to be quite small because r_{tip} is much larger than r_{Al}.

The calculated R_i is summarized in Table IV where several features are recognized. First, the sum of R_i ($0.5837\,\Omega \cdot \text{cm}^2$) is fairly close to that measured in the experiment ($0.69\,\Omega \cdot \text{cm}^2$). The discrepancy is believed to be in the error range, considering the wide variation of the specific contact resistance reported for BSF [31]. To our knowledge, this is also the first time being analytically proved that R_S of (8) is equivalent to that embedded in the light *I–V* curve of the cell. Second, it shows that the spreading resistance ($0.0917\,\Omega \cdot \text{cm}^2$) around the Al finger's tip is appreciable, and can be even larger than the resistance of the rest of the base region ($0.06\,\Omega \cdot \text{cm}^2$). Finally, the resistance of Al finger ($0.25\,\Omega \cdot \text{cm}^2$) appears to be the dominant term of the series resistance. It is caused by the poor electrical conductivity among Al particles owing to the firing and/or paste composition was not optimized. It is possible to reduce Al finger's resistance effectively; for example, improving the connectivity among Al particles with better sintering process, or by printing Ag lines alongside of Al lines. Doing so, FF may gain another 1% absolute as predicted by the empirical equation [32].

Judged with the FF loss mechanism mentioned above, a significant gain of FF is possible by improving both $J_{o,2}$ and R_S. In addition, FF may also be further increased when V_{OC} is improved. Thus, it is quite feasible to have FF over 80% when all are optimized.

IV. CONCLUSION

In summary, IBC and PERC cells have been fabricated on p-type Cz wafers with the industrial process including the screen printing and laser ablation. The IBC cell is demonstrated with the cell efficiency of 20.08%, together with V_{OC} of 645 mV, J_{SC} of 40.15 mA/cm^2, and FF of 77.51%. The efficiency of PERC cell is about 1% lower owing to the much lower J_{SC} (37.83 mA/cm^2). Other than that, V_{OC} and FF of both cells are about the same. The performance of IBC cell has also been verified with the analytical calculation based on the electrical properties measured independently.

In the analysis of V_{OC}, it recognizes the recombination in the n^+-emitter and bulk to be the first two dominant recombination terms. V_{OC} over 700 mV is feasible if both terms are reduced to a negligible level. To achieve, various methods have been proposed including the use of the polysilicon tunneling emitter, thinner wafer with higher bulk lifetime, and improved FFE.

J_{SC} is derived with the electron flux of the p-base being collected by the n^+-emitter. The calculation assumes one-dimensional flux of excess electrons, and results in an excellent estimation of collection loss. The latter can be further reduced with lower S_{eff} of the front surface, higher bulk lifetime, and thinner wafer. The optimal J_{SC} is estimated to be around 41 mA/cm^2 that is not too much different from the value of current IBC cell.

FF is analyzed with the loss caused by $J_{o,2}$ and R_S. The former counts for 3.17% absolute of FF loss, and is attributed to the inappropriate Ag contact firing process. R_S also counts for another 2.94% absolute loss of FF. The high resistivity of Al finger is the dominant term. It has to do with the insufficient electrical connectivity among Al particles in the firing. Both FF losses are process dependent that, when improved, FF over 80% is feasible.

To conclude, a p-Si screen-printed IBC cell, similar to its n-type counterpart, with efficiency up to 22% is readily attainable when V_{OC}, J_{SC}, and FF are all optimized. In addition, PERC cell may perform as well as the IBC cell, provided that any improvement on S_{eff} of the front surface does not compromise the light absorption and emitter resistance of the cell.

REFERENCES

[1] J. Schmidt *et al.*, "Surface passivation of high-efficiency silicon solar cells by atomic-layer-deposited Al_2O_3," *Prog. Photovolt.*, vol. 16, pp. 461–466, Sep. 2008.
[2] T. Dullweber *et al.*, "Towards 20% efficient large-area screen-printed rear-passivated silicon solar cells," *Prog. Photovolt.*, vol. 20, pp. 630–638, Sep. 2012.
[3] B. Hallam *et al.*, "Efficiency enhancement of i-PERC solar cells by implementation of a laser doped selective emitter," *Sol. Energy Mater. Sol. Cells*, vol. 134, pp. 89–98, Mar. 2015.
[4] A. Metz *et al.*, "Industrial high performance crystalline silicon solar cells and modules based on rear surface passivation technology," *Sol. Energy Mater. Sol. Cells*, vol. 120, pp. 417–425, Jan. 2014.

[5] "Trina solar sets 21.25% multicrystalline cell efficiency record," PVTECH, 2015. [Online]. Available: https://www.pv-tech.org/news/trina-solar-sets-new-21.25-multicrystalline-cell-efficiency-record.
[6] "SolarWorld hits 22% PERC efficiency," PV Magazine, 2016. [Online]. Available: https://www.pv-magazine.com/2016/01/14/solarworld-hits-22-perc-efficiency_100022790/.
[7] "Trina sets new mono PERC cell efficiency record of 22.61%," PVTECH, 2016. [Online]. Available: https://www.pv-tech.org/news/trina-sets-new-mono-perc-cell-efficiency-record-of-22.61.
[8] R. Keding *et al.*, "Co-diffused back-contact back-junction silicon solar cells without gap regions," *IEEE J. Photovolt.*, vol. 3, no. 4, pp. 1236–1242, Oct. 2013.
[9] M. Dahlinger *et al.*, "Laser-doped back-contact solar cells," *IEEE J. Photovolt.*, vol. 5, no. 3, pp. 812–818, May 2015.
[10] H. Savin *et al.*, "Black silicon solar cells with interdigitated back-contacts achieve 22.1% efficiency," *Nature Nanotechnol.*, vol. 10, pp. 624–629, Jul. 2015.
[11] D. D. Smith *et al.*, "SunPower's Maxeon Gen III solar cell: High efficiency and energy yield," in *Proc. 2013 IEEE 39th Photovolt. Spec. Conf.*, 2013, pp. 0908–0913.
[12] K. Masuko *et al.*, "Achievement of more than 25% conversion efficiency with crystalline silicon heterojunction solar cell," *IEEE J. Photovolt.*, vol. 4, no. 6, pp. 1433–1435, Nov. 2014.
[13] E. Franklin *et al.*, "Design, fabrication and characterisation of a 24.4% efficient interdigitated back contact solar cell," *Prog. Photovolt.: Res. Appl.*, vol. 24, pp. 411–427, 2016.
[14] "Trina Solar achieves 24.13% conversion efficiency for IBC solar cell," PVTECH, 2017. [Online]. Available: https://www.pv-tech.org/news/trina-solar-achieves-24.13-conversion-efficiency-for-ibc-solar-cell.
[15] R. Woehl, M. Rudiger, D. Biro, and J. Wilde, "All-screen-printed back-contact back-junction silicon solar cells with aluminum-alloyed emitter and demonstration of interconnection of point-shaped metalized contacts," *Prog. Photovolt.*, vol. 23, pp. 226–237, Feb. 2015.
[16] J. Dong *et al.*, "High-efficiency full back contacted cells using industrial processes," *IEEE J. Photovolt.*, vol. 4, no. 1, pp. 130–133, Jan. 2014.
[17] G. Scardera *et al.*, "All-screen-printed dopant paste interdigitated back contact solar cell," *Energy Procedia*, vol. 77, pp. 271–278, 2015.
[18] C. Kranz, J. H. Petermann, T. Dullweber, and R. Brendel, "Simulation-based efficiency gain analysis of 21.2%-efficient screen-printed PERC solar cells," *Energy Procedia*, vol. 92, pp. 109–115, 2016.
[19] R. A. Sinton, A. Cuevas, and M. Stuckings, "Quasi-steady-state photoconductance, a new method for solar cell material and device characterization," in *Proc. 1996 Conf. Rec. 25th IEEE Photovolt. Spec. Conf.*, 1996, pp. 457–460.
[20] C. Honsberg and S. Bowden, PVCDROM. [Online]. Available: http://www.pveducation.org/pvcdrom/characterisation/surface-recombination.
[21] P. Lolgen *et al.*, "Aluminium back-surface field doping profiles with surface recombination velocities below 200 cm/s," in *Proc. 1993 Conf. Rec. 23rd IEEE Photovolt. Spec. Conf.*, 1993, pp. 236–242.
[22] U. Romer *et al.*, "Recombination behavior and contact resistance of n(+) and p(+) poly-crystalline Si/mono-crystalline Si junctions," *Sol. Energy Mater. Sol. Cells*, vol. 131, pp. 85–91, Dec. 2014.
[23] A. D. Upadhyaya *et al.*, "Ion-implanted screen-printed n-type solar cell with tunnel oxide passivated back contact," *IEEE J. Photovolt.*, vol. 6, no. 1, pp. 153–158, Jan. 2016.
[24] C. Reichel, F. Granek, M. Hermle, and S. W. Glunz, "Short-circuit current losses in back-contacted back–junction Si solar cells: Experiment and simulation of the charge collection probability," *IEEE J. Photovolt.*, vol. 3, no. 1, pp. 217–223, Jan. 2013.
[25] C. Reichel, F. Granek, M. Hermle, and S. W. Glunz, "Investigation of electrical shading effects in back-contacted back-junction silicon solar cells using the two-dimensional charge collection probability and the reciprocity theorem," *J. Appl. Phys.*, vol. 109, 2011, Art. no. 024507.
[26] M. M. Hilali, K. Nakayashiki, A. Ebong, and A. Rohatgi, "High-efficiency (19%) screen-printed textured cells on low-resistivity float-zone silicon with high sheet-resistance emitters," *Prog. Photovolt.: Res. Appl.*, vol. 14, pp. 135–144, 2006.
[27] Z. J. Wang *et al.*, "Advanced PERC and PERL production cells with 20.3% record efficiency for standard commercial p-type silicon wafers," *Prog. Photovolt.*, vol. 20, pp. 260–268, May 2012.
[28] C. Honsberg and S. Bowden, PVCDROM. [Online]. Available: http://www.pveducation.org/pvcdrom/characterisation/double-diode-model.
[29] J. Greulich, M. Glatthaar, and S. Rein, "Fill factor analysis of solar cells' current-voltage curves," *Prog. Photovolt.*, vol. 18, pp. 511–515, Nov. 2010.
[30] D. L. Meier and D. K. Schroder, "Contact resistance - Its measurement and relative importance to power loss in a solar-cell," *IEEE Trans. Electron Devices*, vol. 31, no. 6, pp. 647–653, May 1984.
[31] E. Urrejola, K. Peter, H. Plagwitz, and G. Schubert, "Al-Si alloy formation in narrow p-type Si contact areas for rear passivated solar cells," *J. Appl. Phys.*, vol. 107, Jun. 2010, Art. no. 124516.
[32] M. A. Green, "Accuracy of analytical expressions for solar-cell fill factors," *Sol. Cells*, vol. 7, pp. 337–340, 1982.

Authors' photographs and biographies not available at the time of publication.